

Synergistic Conductivity Effect in a Proton Sources-Coupled Metal–Organic Framework

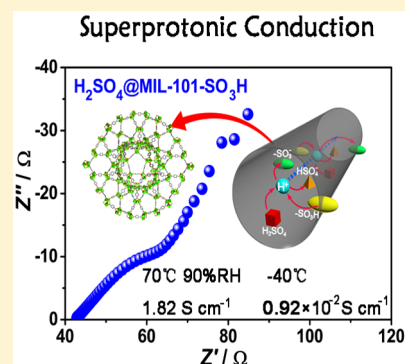
Xiao-Min Li,[†] Long-Zhang Dong,[†] Shun-Li Li,[†] Gang Xu,[‡] Jiang Liu,^{*,†} Feng-Ming Zhang,[†] Li-Shi Lu,[†] and Ya-Qian Lan^{*,†}

[†]Jiangsu Key Laboratory of Biofunctional Materials, School of Chemistry and Materials Science, Nanjing Normal University, Nanjing 210023, PR China

[‡]Fujian Institute of Research on the Structure of Matter, Chinese Academy of Sciences, Fuzhou 350002, PR China

S Supporting Information

ABSTRACT: A water-stable metal–organic framework (MOF)-based composite, $\text{H}_2\text{SO}_4@\text{MIL-101-SO}_3\text{H}$, configured with functionalized sulfonate groups bound to the polymeric backbone and nonvolatile strong acid H_2SO_4 encapsulated into pores, is demonstrated as a superior proton-conducting material, owing to the resultant multiple proton-transfer pathways. This solid material exhibits a superprotonic conductivity of 1.82 S cm^{-1} (70°C , 90% RH) that is comparable to that of other excellent MOF-based proton conductors reported thus far. More importantly, the splendid conductivity ($0.92 \times 10^{-2} \text{ S cm}^{-1}$, -40°C) of the title material achieves an enormous improvement compared with that of all proton-conducting systems demonstrated at subzero temperatures.



Fuel cells as a clean energy resource have attracted considerable attention because of their minimized emission of environmental pollutants and because water is the only byproduct during reaction procedures.¹ To improve the efficiency of fuel cells, electrolyte species^{2–8} displaying high proton conductivity and operating over a wide temperature range are typically required.⁹ Consequently, a wide variety of inorganic or organic compounds,¹⁰ such as ceramic oxides and hydroxides,^{11–13} metal oxides,^{13,14} polymers,^{15,16} oxoacids,^{17,18} and their hybrids/adducts have been well studied as possible proton-conducting materials employed in fuel cells. Among the reported fuel cells systems, the proton-exchange-membrane fuel cell (PEMFC) is recognized as the outstanding substitute for traditional engines as a result of its high power density and ultralow emission features.^{19,20} For instance, the state-of-the-art PEMFC comprises perfluorinated polymer membranes (e.g., Nafion) containing terminal sulfonic acid groups that show high proton conductivity ($10^{-2} \text{ S cm}^{-1}$) in the presence of water and at low temperature ($<80^\circ\text{C}$).²¹ The high cost of the membranes combined with the poor conductivity performance under harsh operating conditions, however, extremely limits its large-scale use in many technologies. Especially for automotive applications, the hydrated PEMs will suffer from severe degradation induced by freeze/thaw cycles when PEMFCs are exposed to subzero temperatures.^{22–24} Currently, very limited progress has been made in this area,^{24–26} though subfreezing operation of fuel cell systems is an important concern. Thus, the development of cheaper and yet better-performing proton-conducting replace-

ments applied to wide temperature range (including subzero temperatures) would be expected for fuel cell applications.

It is well-known that the ionic conductivity is predominantly determined by the amount and mobility of charge carriers (protons),²⁷ regardless of whether electrolyte materials are under hydrous conditions or not. Over recent years, metal–organic frameworks (MOFs) have proved unambiguously to be an excellent platform to obtain advanced proton-conducting materials,^{28–30} because of their intrinsic structural merits, such as well-defined and functionalized pores and channels that are very suitable for forming efficient proton-transfer pathways including various conducting media.^{28,30,31} Another prominent aspect is that the crystalline nature of MOFs can allow direct visualization of the proton hopping and conduction routes, offering valuable insight into structure–property relationships.³² On this foundation, some significant pioneering works by Kitagawa et al.^{33–38} and Shimizu et al.^{27,39–44} have afforded a profound understanding of the proton transportation mechanism, in view of which one can design and synthesize superior conducting materials in a more rational manner. Some practical strategies have now been proposed to introduce multiple proton carriers into MOFs,^{28,29} such as the inclusion of nonvolatile strong acid (H_2SO_4 or H_3PO_4) into pores/channels as well as functionalized moieties (amphiprotic nature) tethered to the

Received: June 28, 2017

Accepted: September 11, 2017



polymeric backbone prone to form potential Brønsted acid–base pairs and hydrogen bonding network, which can greatly promote the proton-conducting properties.^{7,30,37,40,42,44–53} Accordingly, a series of best-performing proton conductors originating from the reported coordination polymers frameworks with aforementioned characters have been explored,^{34,42,48,54} and they continually enhance the application possibilities of the materials.

Considering the feasibility of foregoing tactics, a MIL-101 porous structure derivative [formula given as $\text{Cr}_3(\text{H}_2\text{O})_3\text{O}(\text{BDC}-\text{SO}_3\text{H})_2(\text{BDC}-\text{SO}_3)_2$, MIL-101- SO_3H] possesses functionalized sulfonate groups,⁵⁵ as observed in Nafion, that captured our attention because of its potential proton migration pathway and because it is a proton donor. Also, the high chemical stability of MIL-101- SO_3H likewise allows us to inject H_2SO_4 into its ordered pores and then creates an additional proton-transfer path. In this case, a strong conductivity will probably be anticipated.

In this Letter, a series of $\text{H}_2\text{SO}_4@\text{MIL-101-SO}_3\text{H}$ composite materials loaded with different concentrations of sulfuric acid (1 M, 2 M, and 3 M) are presented that enables a significant rise in conductivity (σ). The detailed conductivity characterization finally confirmed that compound $\text{H}_2\text{SO}_4@\text{MIL-101-SO}_3\text{H}$ (3 M) shows very high σ values of 1.82 S cm^{-1} (70 °C, 90% RH) (Table S1) and $0.92 \times 10^{-2} \text{ S cm}^{-1}$ (−40 °C) (Table S2) for all the MOF-based proton-conducting materials reported to date, and its superior proton conductivity performance under subzero temperature (−40 °C) showed an excellent durability even after 20 hours with a negligible loss of conductivity.

Compound MIL-101- SO_3H with inexpensive raw materials was hydrothermally prepared as previously reported (Supporting Information);⁵⁵ the parent architecture features two types of cages filled with Lewis acidic Cr(III) sites and high-density Brønsted acidic $-\text{SO}_3\text{H}$ sites (Scheme 1a), the latter of which encourage us to explore the proton conductivity, because they can serve as one kind of steady proton source that confers protons to hydrogen-bonded proton-conducting routes. At the same time, different concentrations of aqueous solutions of H_2SO_4 (1 M, 2 M, and 3 M), as another means for releasing protons to the conduction pathways, were blended with the

compound MIL-101- SO_3H , giving rise to our target composite proton-conducting materials $\text{H}_2\text{SO}_4@\text{MIL-101-SO}_3\text{H}$ (Scheme 1b). For the sake of comparison, the parallel $\text{H}_2\text{SO}_4@\text{MIL-101}$ system infused with the same concentrations of H_2SO_4 (1 M, 2 M, and 3 M) and compound MIL-101- SO_3H were tested simultaneously to prove the efficiency of the roles played by the aforementioned two factors in facilitating proton conductivity.

Prior to the proton conductivity characterization, the structural integrity of involved compounds toward treatment of different concentrations of H_2SO_4 solution was confirmed by powder X-ray diffraction (PXRD) analysis. The phase purity of the as-synthesized MIL-101- SO_3H was identified from the PXRD profile which correlated with the pattern for simulated MIL-101. As shown in Figure 1a, the nearly overlapped PXRD

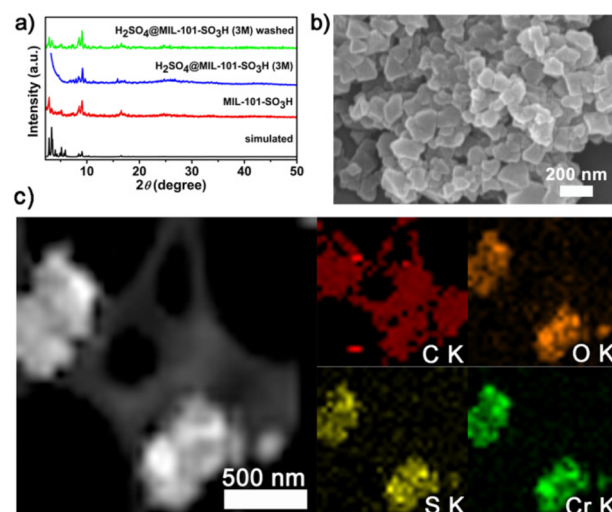
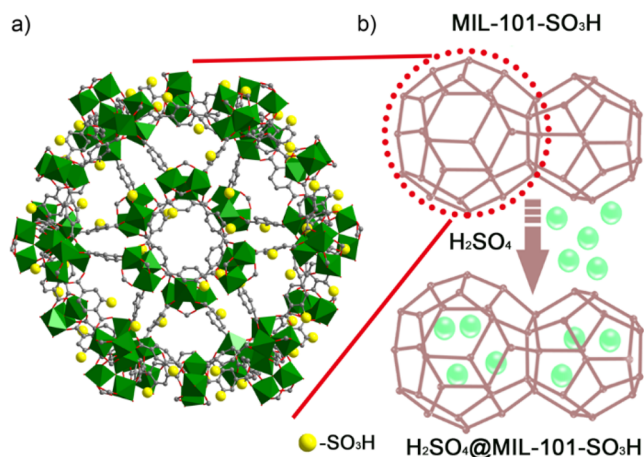


Figure 1. (a) PXRD patterns of simulated MIL-101 (black), as-synthesized MIL-101- SO_3H (red), as-synthesized $\text{H}_2\text{SO}_4@\text{MIL-101-SO}_3\text{H}$ (blue, 3 M), and as-synthesized $\text{H}_2\text{SO}_4@\text{MIL-101-SO}_3\text{H}$ (3 M) washed by water for acid elimination (green). (b) SEM image of as-synthesized $\text{H}_2\text{SO}_4@\text{MIL-101-SO}_3\text{H}$ (3 M). (c) Element mapping images of $\text{H}_2\text{SO}_4@\text{MIL-101-SO}_3\text{H}$ (3 M) suggesting that C, O, S, and Cr elements are in homogeneous distribution.

Scheme 1. (a) Host Framework of Compound MIL-101- SO_3H Decorated with High-Density Brønsted Acidic $-\text{SO}_3\text{H}$ Groups (Yellow Balls) with Green Polyhedron Representing the Coordination Geometry of Cr(III) Spin Center; (b) Schematic Illustration of the Preparation of $\text{H}_2\text{SO}_4@\text{MIL-101-SO}_3\text{H}$ Composite Material



patterns between them are consistent with the scenario documented in ref 55. As for H_2SO_4 -impregnated composite materials, the well-matched PXRD patterns indicated that their parent coordination networks remained intact, albeit with no reflections at lower angles (Figures 1a, S1, and S2), which is likely due to some local distortions and mosaicity of the MIL-101/MIL-101- SO_3H crystal structure upon filling of the pores.⁴⁸ In addition, for the H_2SO_4 -encapsulated sample after washing with water, their PXRD pattern overlapped with that of the original host metal–organic framework (Figures 1a, S1, and S2), further proving the integrity of the host framework. At the same time, measurement of the N_2 adsorption–desorption isotherms of H_2SO_4 -loaded composite materials after washing with water was carried out, as shown in Figures S3b and S4b; the almost overlapped curves further indicate the reservation of structural integrity of pristine host frameworks. Scanning electron microscopy (SEM) images also display that $\text{H}_2\text{SO}_4@\text{MIL-101-SO}_3\text{H}$, MIL-101, and MIL-101- SO_3H have analogous morphologies and grain sizes (Figures 1b, S5, and S6).⁴⁴ It is noted that a trace amount of H_2SO_4 molecules will inevitably attach on the surface of the sample, and it is difficult to dispose of them by washing, as the small H_2SO_4 molecules within large pore spaces

(with the diameters of 1.1 and 1.5 nm) of MIL-101/MIL-101-SO₃H framework also can be removed simultaneously, which has been demonstrated in previous work.⁴⁸ To further confirm H₂SO₄ molecules existed in the pores of MIL-101 and MIL-101-SO₃H networks, N₂ adsorption–desorption isotherm measurements at 77 K were carried out (Figures S3a and S4a). In contrast to the high original isotherms of MIL-101 and MIL-101-SO₃H systems, the dramatically descending uptakes after impregnation of H₂SO₄ solutions suggest that the porous space of host frameworks has been mainly occupied by H₂SO₄ molecules. Moreover, this fact can be confirmed by elemental mapping test whose elemental distributions of C, O, S, and Cr are evenly distributed in the composite material H₂SO₄@MIL-101-SO₃H (3 M) (Figure 1c). In addition, energy-dispersive X-ray spectroscopy (EDX) spectra are shown in Figures S7–S14, where Figures S9–S14 also clearly show the presence of S atoms in H₂SO₄@MIL-101 and H₂SO₄@MIL-101-SO₃H materials. Taking into account these results along with EDX analysis, it is evident that H₂SO₄ molecules were successfully encapsulated into the voids of MIL-101 and MIL-101-SO₃H frameworks.

RH-dependent proton conductivities of the title materials were determined first by using alternating-current (AC) impedance spectroscopy at fixed temperature (30 °C). As we can see, an obviously ascending trend for conductivities of H₂SO₄@MIL-101 (3 M), MIL-101-SO₃H, and H₂SO₄@MIL-101-SO₃H (3 M) has been revealed, with the increasing humidity from 40% to 90% RH. These monotonically increasing plots (Figures S15–S17) highlight that water molecules play an important role in creating the proton-conducting pathways of materials, because it can serve as one kind of proton-transfer vehicle, in the form of H₂O–H₃O⁺. Furthermore, this fact can further be confirmed by the high water adsorption isotherms of these materials executed at 298 K (Figures S18–S21). In addition, sulfonic acid groups make the material more hydrophilic to absorb more water molecules to establish favorable proton-transfer pathways,⁴⁵ similar to those observed in Nafion.⁵⁶ When the humidity rises to 90%, as we can see (Figures S22–S24), the conductivities of targeted materials reach the maximums. The real (*Z'*) and imaginary (*Z''*) parts of the impedance spectra of H₂SO₄@MIL-101 (3 M), MIL-101-SO₃H, H₂SO₄@MIL-101-SO₃H (3 M), and their analogs with different concentrations of H₂SO₄ at 30 °C, 90% RH are shown in Figures 2a,c,e, S25, and S26. The semicircle in the high-frequency region deals with bulk and grain boundary resistance, whereas the tail at low frequency corresponds to mobile ions that are blocked by the electrode–electrolyte interfaces (Figure 2a,c).⁵⁴ As shown in Figure 2e,f, two clear semicircles of MIL-101-SO₃H are present in the high-frequency region, corresponding to the bulk and grain boundary resistance from the contribution of the electrode.⁴⁸ Consequently, we fit the total resistances to calculate the conductivities of the samples. The maximal conductivity ($3.55 \times 10^{-1} \text{ S cm}^{-1}$) of H₂SO₄@MIL-101-SO₃H (3 M) is higher than that of H₂SO₄@MIL-101 (3 M) and more than 4 orders of magnitude above that of MIL-101-SO₃H under the same conditions. Furthermore, such a big σ value exceeds that of any proton-conducting MOF reported to date and the most effective known electrolyte, Nafion (Table S1). The reason for obtaining superprotonic conductivity may be attributed to the synergistic effect of multiple proton units involving water molecules, high acidity of the guest medium (H₂SO₄), and high-density Brønsted acidic –SO₃H groups. In addition, it is undeniable that interparticle phases have a contribution to proton conduction originating from H₂O

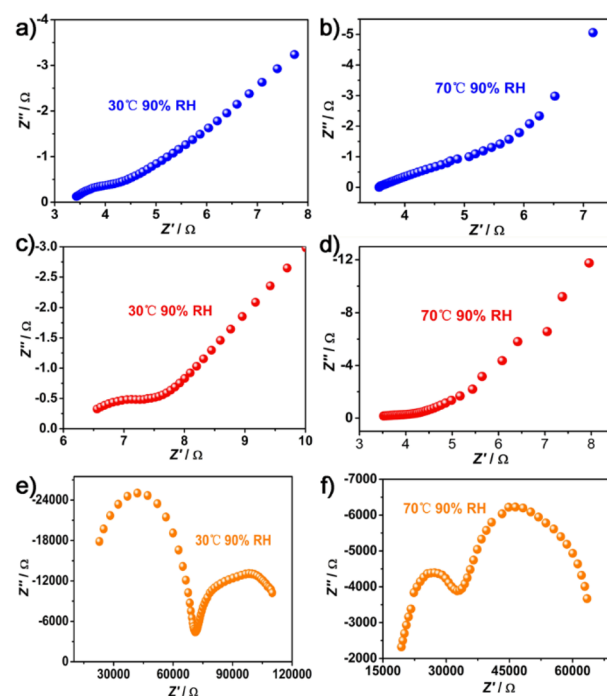


Figure 2. Nyquist plots of (a) H₂SO₄@MIL-101-SO₃H (3 M), (c) H₂SO₄@MIL-101 (3 M), and (e) MIL-101-SO₃H at 30 °C and 90% RH and of (b) H₂SO₄@MIL-101-SO₃H (3 M), (d) H₂SO₄@MIL-101 (3 M), and (f) MIL-101-SO₃H at 70 °C and 90% RH.

molecules and/or a trace of H₂SO₄ molecules on the surface.⁵⁷ To determine further if such a high conductivity for targeted materials can be extended to a wider temperature range, we carried out temperature-dependent conductivity measurements during two heating and cooling cycles with the temperature range of 30–70 °C at 90% RH (Figures S27–S29). The structural integrities of the targeted materials after two heating–cooling cycle measurements have been confirmed by the corresponding PXRD patterns and FT-IR spectra (Figures S30–S32). Upon the elevated temperature, as shown in Figures S33–S35, the conductivity increased steadily. When the temperature ascend to 70 °C, H₂SO₄@MIL-101-SO₃H (3 M), H₂SO₄@MIL-101 (3 M), and MIL-101-SO₃H reached their maximum values of 1.82, 6.09×10^{-1} , and $6.32 \times 10^{-5} \text{ S cm}^{-1}$, respectively (Figure 2b,d,f). Obviously, the high proton conductivity of H₂SO₄@MIL-101-SO₃H (3 M) represents an important breakthrough in MOF-based proton-conductive materials (Table S1). Zview software was used to fit impedance value to get the equivalent circuit at 70 °C and 90% RH (Figure S36). The slight deviations on the conductivities between heating and cooling regime might be related to the different hydrolysis degree of materials, as a result of lacking sufficient time to reabsorb water molecules during the cooling process. Of course, the slower kinetics at lower temperature also has a certain influence for adsorption of water molecules into channels.⁴⁸ In addition, the activation energies (*E_a*) in the cycle tests of materials can be extracted from the relevant Arrhenius plots (Figures S37–S39), which indicated the Grotthuss mechanisms for proton transportation occurred in H₂SO₄@MIL-101-SO₃H (3 M).

The subzero performance of proton-conducting material was deemed as a significant concern in automatic application of fuel cells exposed in colder climates. Therefore, the corresponding conductivity measurements of target materials at lower temper-

atures (-40 to -10 °C) were executed to verify their subfreezing potential as electrolytes. Upon the cooling temperature, there exist a moderate decline in conductivities of $\text{H}_2\text{SO}_4@\text{MIL-101}$ (3 M), $\text{MIL-101-SO}_3\text{H}$, and $\text{H}_2\text{SO}_4@\text{MIL-101-SO}_3\text{H}$ (3 M), as shown in Figure 3c and Table S2. However, the composite

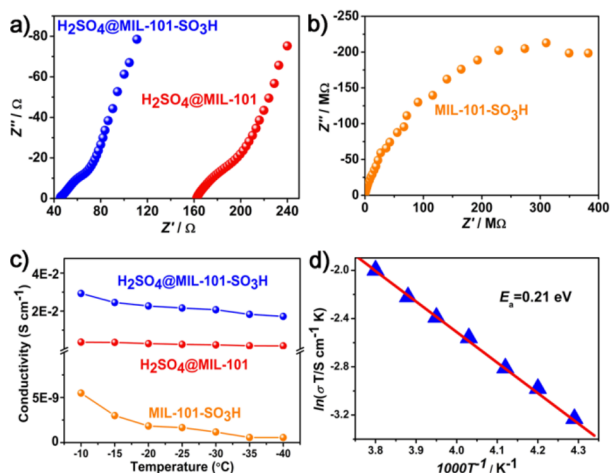


Figure 3. Nyquist plots of (a) $\text{H}_2\text{SO}_4@\text{MIL-101}$ (3 M, red), $\text{H}_2\text{SO}_4@\text{MIL-101-SO}_3\text{H}$ (3 M, blue), and (b) $\text{MIL-101-SO}_3\text{H}$ (orange) at -40 °C. (c) Temperature-dependent proton conductivities of $\text{H}_2\text{SO}_4@\text{MIL-101-SO}_3\text{H}$ (3 M, blue), $\text{H}_2\text{SO}_4@\text{MIL-101}$ (3 M, red), and $\text{MIL-101-SO}_3\text{H}$ (orange). (d) Arrhenius plots of $\text{H}_2\text{SO}_4@\text{MIL-101-SO}_3\text{H}$ (3 M) at subzero temperatures. The solid line (red) is shown to calculate the value of E_a .

$\text{H}_2\text{SO}_4@\text{MIL-101-SO}_3\text{H}$ (3 M) still maintains a high value of σ ($0.92 \times 10^{-2} \text{ S cm}^{-1}$) at -40 °C, which is the highest among all the reported proton-conducting materials at subzero temperature (Table S3). From the temperature-dependent plots of conductivity (Figure 3c), $\text{H}_2\text{SO}_4@\text{MIL-101-SO}_3\text{H}$ (3 M) composite performs much better than $\text{H}_2\text{SO}_4@\text{MIL-101}$ (3 M) and $\text{MIL-101-SO}_3\text{H}$, which benefited from the effective combination of two kinds of protonic sources. Moreover, the Nyquist plots related to the title materials indicate that the conductivity was indeed promoted tremendously by enduring higher concentration of H_2SO_4 molecules compatible with the host framework (Figures 3a,b, S40, and S41). Given that keeping good performance in cooling–heating cycles is necessary for fuel cell application, the cyclic measurements to the conductivities of $\text{H}_2\text{SO}_4@\text{MIL-101}$ (3 M), $\text{MIL-101-SO}_3\text{H}$, and $\text{H}_2\text{SO}_4@\text{MIL-101-SO}_3\text{H}$ (3 M) were separately performed two times (Figures S42–S44). The final structural robustness of the title materials after measurements were confirmed by matched PXRD patterns and FT-IR spectra (Figures S45–S47). Apparently, the cooling conductivity plots of these materials (Figures S48–S50) were almost linear, showing no significant transformations in the sample hydration.⁴⁸ At the same time, the altered temperature has hardly affected the acid content because of the observed minor variation of conductivity values (Figures S48 and S50) which reveal the predictable nature of conductivity patterns that are beneficial for possible fuel cell application. In the cycle measurements, each material under this condition was pressed into three samples to get individually corresponding resistance values, and then we use their average resistance (R'_{average}) to calculate E_a values to get a better linear relationship and more accurate E_a values. The activation energies (E_a) extracted from the Arrhenius equation for $\text{H}_2\text{SO}_4@\text{MIL-101}$ (3 M), $\text{MIL-101-SO}_3\text{H}$, and $\text{H}_2\text{SO}_4@\text{MIL-101-SO}_3\text{H}$ (3 M) are shown in Figures

S51, S52, and S53, respectively, wherein the energy values of $\text{H}_2\text{SO}_4@\text{MIL-101-SO}_3\text{H}$ (3 M) and $\text{H}_2\text{SO}_4@\text{MIL-101}$ (3 M) are much lower than that of $\text{MIL-101-SO}_3\text{H}$, suggesting the introduction of H_2SO_4 with low pK_a value into $\text{MIL-101}/\text{MIL-101-SO}_3\text{H}$ skeleton provides more protons that are conducive for efficient proton transportation. The activation energy (E_a) shown in Figure 3d was extracted from the first cooling cycle of $\text{H}_2\text{SO}_4@\text{MIL-101-SO}_3\text{H}$ (3 M). The small E_a value (0.21 eV) lies within the range corresponding to the Grotthuss mechanism,⁵⁸ which involves fast proton transfer between adjacent $\text{H}_2\text{SO}_4 \cdots \text{HSO}_4^-$ and/or $-\text{SO}_3\text{H} \cdots -\text{SO}_3^-$ Brønsted acid–base pairs. Such lower value of activation energy for proton transfer was also reported in other high acid-encapsulated proton-conducting materials.^{48,49,59} In addition, the discrepancy in the proton conductivity of the involved materials between ambient atmosphere and subzero temperature is probably ascribed to the reduced hydration level caused by water molecules freezing. In order to further validate the reliability of conductivity of materials at subzero temperatures, time-dependent proton conductivity measurements of $\text{H}_2\text{SO}_4@\text{MIL-101-SO}_3\text{H}$ (3 M) were performed at -40 °C. Remarkably, high proton conductivity with a negligible loss was conserved even after 20 hours (Figure S54), and the corresponding PXRD pattern and FT-IR spectra finally corroborated the structural integrity of the composite (Figure S55), suggesting an excellent durability of composite $\text{H}_2\text{SO}_4@\text{MIL-101-SO}_3\text{H}$ (3 M).

Efficient proton-transfer pathways are integral to proton conduction, which is germane to hydrogen-bonded network.^{29,30} The intrinsic proton-conducting mechanism of the investigated composite materials (Figure 4) demonstrates that the high

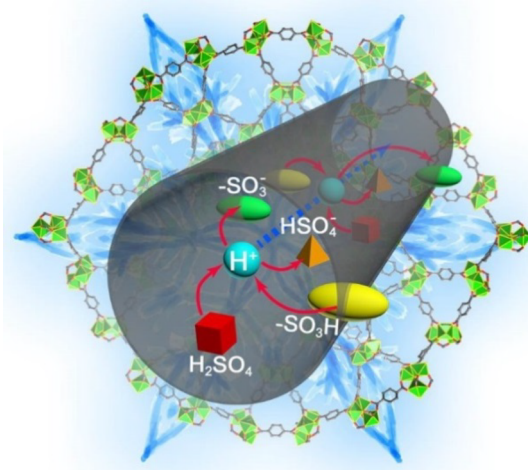


Figure 4. Schematic view of possible intrinsic proton conduction mechanism for $\text{H}_2\text{SO}_4@\text{MIL-101-SO}_3\text{H}$ including proton donors (H_2SO_4 molecules and $-\text{SO}_3\text{H}$ groups), proton receivers (HSO_4^- and $-\text{SO}_3^-$ ions), and proton carriers (H^+ ion).

conductivity partially rests upon the hydrogen-bonded network contributed by $\text{H}_2\text{SO}_4-\text{HSO}_4^-$ acid–base pair in which H_2SO_4 is regarded as proton donor to form an efficient proton-transfer pathway in pores. As the increased content of H_2SO_4 (based on S/Cr atomic ratios calculated from EDS results, as shown in Tables S4 and S5) molecules in $\text{MIL-101}/\text{MIL-101-SO}_3\text{H}$, the corresponding proton conductivities of the title compounds at indicated temperatures were improved clearly. In addition, the sulfonate acid groups of $\text{MIL-101-SO}_3\text{H}$ can also provide protons to increase proton carriers, and it can function to deliver

water molecules nearby into the pores to form efficient proton-transfer pathways, resulting in a large improvement on proton conduction. From the comparison of activation energies at the indicated temperature range (-40 to 70 °C) (Table S6), the coexistence of three types of proton sources (H_2O , H_2SO_4 , and $-\text{SO}_3\text{H}^-$) resulted in multiple possibilities of proton transport referring to Grotthuss and vehicular mechanisms, while the Grotthuss mechanism became even more dominant for $\text{H}_2\text{SO}_4@ \text{MIL-101-SO}_3\text{H}$ (3 M)/ $\text{H}_2\text{SO}_4@ \text{MIL-101}$ (3 M) in subzero temperatures. Attempts to perform theoretical calculation so as to have a full understanding of the specific proton conductive paths occurring in these materials have proven unsuccessful because of the great number of atoms within the unit cell of host MOF framework resulting in an unimaginably complicated computation.

In summary, we have fabricated a superior conductive composite $\text{H}_2\text{SO}_4@ \text{MIL-101-SO}_3\text{H}$ that displays efficient multifold proton-transfer pathways contributed by water molecules (hydrous condition), functionalized sulfonate groups tethered to the polymeric backbone, and nonvolatile strong acid (H_2SO_4) encapsulated into pores. The simple and viable composite approach finally endows target material with superprotonic conductivities of 1.82 S cm^{-1} (70 °C, 90% RH) and $0.92 \times 10^{-2} \text{ S cm}^{-1}$ (-40 °C), both of which have surpassed that of any MOF-based proton conductors reported to date, on equal terms. Moreover, such high conductivity can be retained for at least 20 h under -40 °C, indicative of excellent structural stability under harsh fuel cell operating conditions. The prominent performance on proton conductivity of $\text{H}_2\text{SO}_4@ \text{MIL-101-SO}_3\text{H}$ is mainly attributed to the synergistic effect of multiple effective proton units. At the same time, our findings should also arouse more research interest in further improvement of commercial solid electrolytes or proton sensors.

■ ASSOCIATED CONTENT

■ Supporting Information

The Supporting Information is available free of charge on the ACS Publications website at DOI: 10.1021/acsenergylett.7b00560.

Detailed information regarding the experimental methods, related materials' characterization, and proton conduction performance (PDF)

■ AUTHOR INFORMATION

Corresponding Authors

*E-mail: yqlan@njnu.edu.cn.

*E-mail: liuj0828@163.com.

ORCID

Long-Zhang Dong: 0000-0002-9276-5101

Feng-Ming Zhang: 0000-0002-2738-306X

Ya-Qian Lan: 0000-0002-2140-7980

Notes

The authors declare no competing financial interest.

■ ACKNOWLEDGMENTS

This work was financially supported by the National Natural Science Foundation of China (Nos. 21622104, 21371099, and 21471080), the NSF of Jiangsu Province of China (No. BK20141445), the Priority Academic Program Development of Jiangsu Higher Education Institutions, and the Foundation of

Jiangsu Collaborative Innovation Center of Biomedical Functional Materials.

■ REFERENCES

- (1) Winter, M.; Brodd, R. J. What Are Batteries, Fuel Cells, and Supercapacitors? *Chem. Rev.* **2004**, *104*, 4245–4270.
- (2) Wang, H.; Xu, X.; Johnson, N. M.; Dandala, N. K. R.; Ji, H. F. High Proton Conductivity of Water Channels in a Highly Ordered Nanowire. *Angew. Chem., Int. Ed.* **2011**, *50*, 12538–12541.
- (3) Borges, D. D.; Devautour-Vinot, S.; Jobic, H.; Ollivier, J.; Nouar, F.; Semino, R.; Devic, T.; Serre, C.; Paesani, F.; Maurin, G. Proton Transport in a Highly Conductive Porous Zirconium-Based Metal–Organic Framework: Molecular Insight. *Angew. Chem.* **2016**, *128*, 3987–3992.
- (4) Karmakar, A.; Illathvalappil, R.; Anothumakkool, B.; Sen, A.; Samanta, P.; Desai, A. V.; Kurungot, S.; Ghosh, S. K. Hydrogen-Bonded Organic Frameworks (HOFs): A New Class of Porous Crystalline Proton-Conducting Materials. *Angew. Chem.* **2016**, *128*, 10825–10829.
- (5) Ma, H.; Liu, B.; Li, B.; Zhang, L.; Li, Y.-G.; Tan, H.-Q.; Zang, H.-Y.; Zhu, G. Cationic Covalent Organic Frameworks: A Simple Platform of Anionic Exchange for Porosity Tuning and Proton Conduction. *J. Am. Chem. Soc.* **2016**, *138*, 5897–5903.
- (6) Vilčiauskas, L.; Tuckerman, M. E.; Bester, G.; Paddison, S. J.; Kreuer, K.-D. The mechanism of proton conduction in phosphoric acid. *Nat. Chem.* **2012**, *4*, 461–466.
- (7) Bureekaew, S.; Horike, S.; Higuchi, M.; Mizuno, M.; Kawamura, T.; Tanaka, D.; Yanai, N.; Kitagawa, S. One-dimensional imidazole aggregate in aluminium porous coordination polymers with high proton conductivity. *Nat. Mater.* **2009**, *8*, 831–836.
- (8) Xu, H.; Tao, S.; Jiang, D. Proton conduction in crystalline and porous covalent organic frameworks. *Nat. Mater.* **2016**, *15*, 722–726.
- (9) Kreuer, K.-D.; Paddison, S. J.; Spohr, E.; Schuster, M. Transport in Proton Conductors for Fuel-Cell Applications: Simulations, Elementary Reactions, and Phenomenology. *Chem. Rev.* **2004**, *104*, 4637–4678.
- (10) Akutsu-Sato, A.; Akutsu, H.; Turner, S. S.; Day, P.; Probert, M. R.; Howard, J. A. K.; Akutagawa, T.; Takeda, S.; Nakamura, T.; Mori, T. The First Proton-Conducting Metallic Ion-Radical Salts. *Angew. Chem., Int. Ed.* **2005**, *44*, 292–295.
- (11) Iwahara, H. Proton conducting ceramics and their applications. *Solid State Ionics* **1996**, *86*, 9–15.
- (12) Wang, S.; Zhao, F.; Zhang, L.; Chen, F. Synthesis of $\text{BaCe}_{0.7}\text{Zr}_{0.1}\text{Yb}_{0.1}\text{O}_{3-\delta}$ proton conducting ceramic by a modified Pechini method. *Solid State Ionics* **2012**, *213*, 29–35.
- (13) Kreuer, K. D. Proton-conducting oxides. *Annu. Rev. Mater. Res.* **2003**, *33*, 333–359.
- (14) Iwahara, H.; Uchida, H.; Ono, K.; Ogaki, K. Proton Conduction in Sintered Oxides Based on BaCeO_3 . *J. Electrochem. Soc.* **1988**, *135*, 529–533.
- (15) Schuster, M. F. H.; Meyer, W. H.; Schuster, M.; Kreuer, K. D. Toward a New Type of Anhydrous Organic Proton Conductor Based on Immobilized Imidazole. *Chem. Mater.* **2004**, *16*, 329–337.
- (16) Schuster, M. F. H.; Meyer, W. H. Anhydrous proton-conducting polymers. *Annu. Rev. Mater. Res.* **2003**, *33*, 233–261.
- (17) Vilčiauskas, L.; de Araujo, C. C.; Kreuer, K.-D. Proton conductivity and diffusion in molten phosphinic acid (H_3PO_2): The last member of the phosphorus oxoacid proton conductor family. *Solid State Ionics* **2012**, *212*, 6–9.
- (18) Boysen, D. A.; Uda, T.; Chisholm, C. R. I.; Haile, S. M. High-Performance Solid Acid Fuel Cells Through Humidity Stabilization. *Science* **2004**, *303*, 68.
- (19) Murphy, O. J.; Hitchens, G. D.; Manko, D. J. High power density proton-exchange membrane fuel cells. *J. Power Sources* **1994**, *47*, 353–368.
- (20) Prater, K. B. Solid polymer fuel cells for transport and stationary applications. *J. Power Sources* **1996**, *61*, 105–109.
- (21) Paddison, S. J. Proton Conduction Mechanisms at Low Degrees of Hydration in Sulfonic Acid–Based Polymer Electrolyte Membranes. *Annu. Rev. Mater. Res.* **2003**, *33*, 289–319.

- (22) Song, M.-K.; Li, H.; Li, J.; Zhao, D.; Wang, J.; Liu, M. Tetrazole-based, Anhydrous Proton Exchange Membranes for Fuel Cells. *Adv. Mater.* **2014**, *26*, 1277–1282.
- (23) Kim, S.; Mench, M. M. Physical degradation of membrane electrode assemblies undergoing freeze/thaw cycling: Micro-structure effects. *J. Power Sources* **2007**, *174*, 206–220.
- (24) Yan, Q.; Toghiani, H.; Lee, Y.-W.; Liang, K.; Causey, H. Effect of sub-freezing temperatures on a PEM fuel cell performance, startup and fuel cell components. *J. Power Sources* **2006**, *160*, 1242–1250.
- (25) Ye, Y.; Zhang, L.; Peng, Q.; Wang, G.-E.; Shen, Y.; Li, Z.; Wang, L.; Ma, X.; Chen, Q.-H.; Xiang, S.; et al. High Anhydrous Proton Conductivity of Imidazole-Loaded Mesoporous Polyimides over a Wide Range from Subzero to Moderate Temperature. *J. Am. Chem. Soc.* **2015**, *137*, 913–918.
- (26) Ye, Y.; Wu, X.; Yao, Z.; Wu, L.; Cai, Z.; Wang, L.; Ma, X.; Chen, Q.-H.; Zhang, Z.; Xiang, S. Metal-organic frameworks with a large breathing effect to host hydroxyl compounds for high anhydrous proton conductivity over a wide temperature range from subzero to 125°C. *J. Mater. Chem. A* **2016**, *4*, 4062–4070.
- (27) Shimizu, G. K. H.; Taylor, J. M.; Kim, S. Proton Conduction with Metal–Organic Frameworks. *Science* **2013**, *341*, 354.
- (28) Ramaswamy, P.; Wong, N. E.; Shimizu, G. K. H. MOFs as proton conductors - challenges and opportunities. *Chem. Soc. Rev.* **2014**, *43*, 5913–5932.
- (29) Yamada, T.; Otsubo, K.; Makiura, R.; Kitagawa, H. Designer coordination polymers: dimensional crossover architectures and proton conduction. *Chem. Soc. Rev.* **2013**, *42*, 6655–6669.
- (30) Yoon, M.; Suh, K.; Natarajan, S.; Kim, K. Proton Conduction in Metal–Organic Frameworks and Related Modularly Built Porous Solids. *Angew. Chem., Int. Ed.* **2013**, *52*, 2688–2700.
- (31) Canivet, J.; Fateeva, A.; Guo, Y.; Coasne, B.; Farrusseng, D. Water adsorption in MOFs: fundamentals and applications. *Chem. Soc. Rev.* **2014**, *43*, 5594–5617.
- (32) Sahoo, S. C.; Kundu, T.; Banerjee, R. Helical Water Chain Mediated Proton Conductivity in Homochiral Metal–Organic Frameworks with Unprecedented Zeolitic unh-Topology. *J. Am. Chem. Soc.* **2011**, *133*, 17950–17958.
- (33) Sadakiyo, M.; Yamada, T.; Kitagawa, H. Rational Designs for Highly Proton-Conductive Metal–Organic Frameworks. *J. Am. Chem. Soc.* **2009**, *131*, 9906–9907.
- (34) Yamada, T.; Sadakiyo, M.; Kitagawa, H. High Proton Conductivity of One-Dimensional Ferrous Oxalate Dihydrate. *J. Am. Chem. Soc.* **2009**, *131*, 3144–3145.
- (35) Sadakiyo, M.; Ōkawa, H.; Shigematsu, A.; Ohba, M.; Yamada, T.; Kitagawa, H. Promotion of Low-Humidity Proton Conduction by Controlling Hydrophilicity in Layered Metal–Organic Frameworks. *J. Am. Chem. Soc.* **2012**, *134*, 5472–5475.
- (36) Sadakiyo, M.; Yamada, T.; Honda, K.; Matsui, H.; Kitagawa, H. Control of Crystalline Proton-Conducting Pathways by Water-Induced Transformations of Hydrogen-Bonding Networks in a Metal–Organic Framework. *J. Am. Chem. Soc.* **2014**, *136*, 7701–7707.
- (37) Shigematsu, A.; Yamada, T.; Kitagawa, H. Wide Control of Proton Conductivity in Porous Coordination Polymers. *J. Am. Chem. Soc.* **2011**, *133*, 2034–2036.
- (38) Bao, S.-S.; Otsubo, K.; Taylor, J. M.; Jiang, Z.; Zheng, L.-M.; Kitagawa, H. Enhancing Proton Conduction in 2D Co–La Coordination Frameworks by Solid-State Phase Transition. *J. Am. Chem. Soc.* **2014**, *136*, 9292–9295.
- (39) Hurd, J. A.; Vaidhyanathan, R.; Thangadurai, V.; Ratcliffe, C. I.; Moudrakovski, I. L.; Shimizu, G. K. H. Anhydrous proton conduction at 150°C in a crystalline metal–organic framework. *Nat. Chem.* **2009**, *1*, 705–710.
- (40) Kim, S.; Dawson, K. W.; Gelfand, B. S.; Taylor, J. M.; Shimizu, G. K. H. Enhancing Proton Conduction in a Metal–Organic Framework by Isomorphous Ligand Replacement. *J. Am. Chem. Soc.* **2013**, *135*, 963–966.
- (41) Ramaswamy, P.; Wong, N. E.; Gelfand, B. S.; Shimizu, G. K. H. A Water Stable Magnesium MOF That Conducts Protons over 10^{−2} S cm^{−1}. *J. Am. Chem. Soc.* **2015**, *137*, 7640–7643.
- (42) Taylor, J. M.; Dawson, K. W.; Shimizu, G. K. H. A Water-Stable Metal–Organic Framework with Highly Acidic Pores for Proton-Conducting Applications. *J. Am. Chem. Soc.* **2013**, *135*, 1193–1196.
- (43) Taylor, J. M.; Mah, R. K.; Moudrakovski, I. L.; Ratcliffe, C. I.; Vaidhyanathan, R.; Shimizu, G. K. H. Facile Proton Conduction via Ordered Water Molecules in a Phosphonate Metal–Organic Framework. *J. Am. Chem. Soc.* **2010**, *132*, 14055–14057.
- (44) Umeyama, D.; Horike, S.; Inukai, M.; Hijikata, Y.; Kitagawa, S. Confinement of Mobile Histamine in Coordination Nanochannels for Fast Proton Transfer. *Angew. Chem., Int. Ed.* **2011**, *50*, 11706–11709.
- (45) Phang, W. J.; Jo, H.; Lee, W. R.; Song, J. H.; Yoo, K.; Kim, B.; Hong, C. S. Superprotonic Conductivity of a UiO-66 Framework Functionalized with Sulfonic Acid Groups by Facile Postsynthetic Oxidation. *Angew. Chem., Int. Ed.* **2015**, *54*, 5142–5146.
- (46) Pili, S.; Argent, S. P.; Morris, C. G.; Rought, P.; García-Sakai, V.; Silverwood, I. P.; Easun, T. L.; Li, M.; Warren, M. R.; Schröder, M.; et al. Proton Conduction in a Phosphonate-Based Metal–Organic Framework Mediated by Intrinsic “Free Diffusion inside a Sphere”. *J. Am. Chem. Soc.* **2016**, *138*, 6352–6355.
- (47) Umeyama, D.; Horike, S.; Inukai, M.; Kitagawa, S. Integration of Intrinsic Proton Conduction and Guest-Accessible Nanospace into a Coordination Polymer. *J. Am. Chem. Soc.* **2013**, *135*, 11345–11350.
- (48) Ponomareva, V. G.; Kovalenko, K. A.; Chupakhin, A. P.; Dybtsev, D. N.; Shutova, E. S.; Fedin, V. P. Imparting High Proton Conductivity to a Metal–Organic Framework Material by Controlled Acid Impregnation. *J. Am. Chem. Soc.* **2012**, *134*, 15640–15643.
- (49) Dybtsev, D. N.; Ponomareva, V. G.; Aliev, S. B.; Chupakhin, A. P.; Gallyamov, M. R.; Moroz, N. K.; Kolesov, B. A.; Kovalenko, K. A.; Fedin, V. P.; et al. High Proton Conductivity and Spectroscopic Investigations of Metal–Organic Framework Materials Impregnated by Strong Acids. *ACS Appl. Mater. Interfaces* **2014**, *6*, 5161–5167.
- (50) Chandra, S.; Kundu, T.; Dey, K.; Addicoat, M.; Heine, T.; Banerjee, R. Interplaying Intrinsic and Extrinsic Proton Conductivities in Covalent Organic Frameworks. *Chem. Mater.* **2016**, *28*, 1489–1494.
- (51) Chandra, S.; Kundu, T.; Kandambeth, S.; Baba Rao, R.; Marathe, Y.; Kunjir, S. M.; Banerjee, R. Phosphoric Acid Loaded Azo (–N=N–) Based Covalent Organic Framework for Proton Conduction. *J. Am. Chem. Soc.* **2014**, *136*, 6570–6573.
- (52) Tezuka, T.; Tadanaga, K.; Hayashi, A.; Tatsumisago, M. Inorganic–Organic Hybrid Membranes with Anhydrous Proton Conduction Prepared from 3-Aminopropyltriethoxysilane and Sulfuric Acid by the Sol–Gel Method. *J. Am. Chem. Soc.* **2006**, *128*, 16470–16471.
- (53) Taylor, J. M.; Komatsu, T.; Dekura, S.; Otsubo, K.; Takata, M.; Kitagawa, H. The Role of a Three Dimensionally Ordered Defect Sublattice on the Acidity of a Sulfonated Metal–Organic Framework. *J. Am. Chem. Soc.* **2015**, *137*, 11498–11506.
- (54) Nagarkar, S. S.; Unni, S. M.; Sharma, A.; Kurungot, S.; Ghosh, S. K. Two-in-One: Inherent Anhydrous and Water-Assisted High Proton Conduction in a 3D Metal–Organic Framework. *Angew. Chem., Int. Ed.* **2014**, *53*, 2638–2642.
- (55) Zhou, Y.-X.; Chen, Y.-Z.; Hu, Y.; Huang, G.; Yu, S.-H.; Jiang, H.-L. MIL-101-SO₃H: A Highly Efficient Brønsted Acid Catalyst for Heterogeneous Alcoholysis of Epoxides under Ambient Conditions. *Chem. - Eur. J.* **2014**, *20*, 14976–14980.
- (56) Slade, R. C. T.; Hardwick, A.; Dickens, P. G. Investigation of H⁺ motion in NAFION film by pulsed 1H NMR and A.C. conductivity measurements. *Solid State Ionics* **1983**, *9*, 1093–1098.
- (57) Tominaka, S.; Cheetham, A. K. Intrinsic and extrinsic proton conductivity in metal-organic frameworks. *RSC Adv.* **2014**, *4*, 54382–54387.
- (58) Kreuer, K.-D. Proton Conductivity: Materials and Applications. *Chem. Mater.* **1996**, *8*, 610–641.
- (59) Nakamura, O.; Kodama, T.; Ogino, I.; Miyake, Y. High-Conductivity Solid Proton Conductors: Dodecamolybdophosphoric Acid and Dodecatungstophosphoric Acid Crystals. *Chem. Lett.* **1979**, *8*, 17–18.